SCIENCE CHINA
Physics, Mechanics & Astronomy

• Research Paper •

April 2010 Vol.53 No.4: 699–711
doi: 10.1007/s11433-010-0169-z

A constitutive model of frozen soil with damage and numerical simulation for the coupled problem

ZHU ZhiWu[1], NING JianGuo[2*] & MA Wei[3]

[1] *School of Mechanics and Engineering, Southwest Jiaotong University, Chengdu 610031, China;*
[2] *State Key Laboratory of Explosion Science and Technology, Beijing Institute of Technology, Beijing 100081, China;*
[3] *Key Laboratory of Frozen Soil Engineering, CAREERI, CAS, Lanzhou 730000, China*

Received January 6, 2010; accepted February 23, 2010

Based on the microcosmic mechanics of composite materials, an elastic constitutive model for frozen soil with damage is presented. For frozen sandy soil with a range of ice contents and under a range of temperature conditions, quantitative results determined by this constitutive model agree with practically measured stress-strain curves. After numerically simulating the coupled water, temperature and stress fields of channel frozen and frozen roadbed using a self-developed finite-element routine, more accurate and practical calculation results for the temperature field coupled with stress, displacement and strain fields are obtained; the results match predictions and tests undertaken by earlier researchers. Our results support the reliability of our routine for calculating interdependent physical quantities of frozen soil and for describing the relationships between them. Our program can offer necessary constraints for engineering design and construction in permafrost regions.

frozen soil, microcosmic mechanics, roadbed, coupling, stress field

PACS: 92.40.Lg, 62.20.Fe, 83.10.Gr

1 Introduction

Frozen soil is a kind of composite materials composed of soil particles, ice, unfrozen water and gas. The rheological properties of the ice make the mechanical properties of frozen soil very different from the common soil. The mechanical properties of frozen soil are influenced by the soil type, pressure and temperature. due to the unfrozen water and ice existing in the frozen soil. The physical and mechanical properties of the whole frozen soil are affected by each component when their types and contents change.

The strength characteristics of frozen soil are fundamental to foundation and structural design in cold region construction. Previous investigations into the characteristics of frozen soil and ice-soil interactions have focused on developing mechanical models under either thermodynamic or mixture theories. For example, Fremond [1] pioneered the description of the thermodynamics properties of frozen soil. Gary [2] systematically analyzed heat transmission during the melting of frozen soil. Konard [3] presented a model that could describe ice formation and moisture movement in the soil freezing process. Dennis [4] systematically investigated the process of freezing. A more thorough experimental study and theoretical analysis has been done by An [5] et al. on water migration, heat and mass transfer, water-temperature-stress coupling and the determination of constitutive equations of frozen soil. However, most of the former research focused on developing mechanical models based on either thermodynamics or mixture theories and determining the coupling temperature field and water field.

Frozen soil causes many engineering problems for the construction of highways, railways, and oil pipelines in cold regions. Investigations of the mechanisms that result in frost damage address several aspects of this problem. Foriero [6]

*Corresponding author (email: jgning@bit.edu.cn)

et al. simulated the down-slope creep of frozen soil with a finite element method. Su [7] et al. utilized an elastic finite element method to model creep properties of frozen soil. Dempsey [8] established a prognostic model of water and heat coupled in unsaturated soil. Rai [9] derived a governing differential equation for fully coupled fluid, heat flow and soil deformation, and provided an analytical solution based on double porosity and a multihole thermodynamics formula. Given initial unknown quantities for displacement, pore pressure and humidity, Masters [10] investigated the regularity of the coupling for soil body deformation, fluid temperature and pore pressure. Zhang [11] et al. undertook a nonlinear analysis of a two-variable coupling problem for the temperature field and seepage field in a cold-environment tunnel. Later, they expanded their analysis to a three-variable coupling problem for the temperature field, seepage field and stress field. However, to date there is still no reliable software that incorporates frozen soil in the numerical simulation.

This paper studies the coupled mechanical problem of frozen soils that involves pore water combined with thermal and stress fields. From an examination of the microcosmic mechanics of the composite material, a new constitutive model for soil containing frost damage is established. The mathematics that governs the coupling problem of temperature, water and stress fields is developed according to heat transfer theory, seepage theory and the mechanics of frozen soil. The corresponding numerical simulations that determine expressions for the temperature, water and stress fields are developed by a finite-element routine.

2 A constitutive model of frozen soil with damage

2.1 The elastic modulus of frozen soil

Frozen soil, from the viewpoint of the complexity of its inner structure, can initially be regarded as a compound consisting solely of soil and ice, temporarily ignoring the effects of water and porosity. Soil grains constitute the framework of composite material, whereas ice is regarded as the filler; this enables the development of a constitutive relationship by using the mixing law of composite material theory. Frost damage effects can then be considered. Suppose the soil particles within frozen soil are even and continuous and the soil particles bond with ice completely. E_s and E_i are taken as the elastic moduli of soil and ice, respectively; similarly G_s and G_i are the shear moduli, and ν_s and ν_i are the Poisson's ratios. The subscripts *s* and *i* denote the components of soil and ice in frozen soil respectively. Hence the equivalent elastic modulus *K* and the equivalent shear modulus *G* of frozen soil are obtained according to the microcosmic mechanics mixing law:

$$K = \varphi\left(K_s, K_i\right), \tag{1}$$

$$G = \phi\left(G_s, G_i\right). \tag{2}$$

Based on the relationship between the elastic constants of isotropic materials: $K = E/3(1-2\nu)$, $G = E/2(1+\nu)$, the equivalent elastic modulus E and the equivalent Poisson's ratio ν of frozen soil can be written with the equations mentioned above [12]:

$$E = \frac{\left[c_s E_s\left(1-2\nu_i\right)+c_i E_i\left(1-2\nu_s\right)\right]\left[c_s E_s\left(1+\nu_i\right)+c_i E_i\left(1+\nu_s\right)\right]}{c_s E_s\left(1+\nu_i\right)\left(1-2\nu_i\right)+c_i E_i\left(1+\nu_s\right)\left(1-2\nu_s\right)}, \tag{3}$$

$$\nu = \frac{c_s E_s \nu_s\left(1+\nu_i\right)\left(1-2\nu_i\right)+c_i E_i \nu_i\left(1+\nu_s\right)\left(1-2\nu_s\right)}{c_s E_s\left(1+\nu_i\right)\left(1-2\nu_i\right)+c_i E_i\left(1+\nu_s\right)\left(1-2\nu_s\right)}, \tag{4}$$

where c_s and c_i are the soil volumetric content (also called volume fraction) and ice volumetric content respectively.

2.2 The constitutive relationship of frozen soil with damage

According to Lemaitre's equivalent stress principle [13], the strain caused by σ acting on the damaged material is equivalent to the strain caused by $\tilde{\sigma}$ acting on the undamaged material. The stress-strain relationship of damaged frozen soil under the one-dimensional condition can be written as

$$\varepsilon = \frac{\sigma}{\tilde{E}} = \frac{\tilde{\sigma}}{E} = \frac{\sigma}{E(1-D)}, \tag{5}$$

where $\tilde{\sigma}$ is the equivalent stress in damage mechanics, and is equal to effective stress in soil mechanics, E is the elastic modulus of the undamaged material, i.e., the initial elastic modulus determined by eq. (3), $\tilde{E}$ is the elastic modulus of the damaged material, i.e., the effective elastic modulus, and D is the damage quantity.

Consequently, according to damage mechanics [14], the constitutive relationship for damaged material $(D \neq 0)$ can be derived from the constitutive equation for undamaged material $(D = 0)$. This means that the nominal stress, which is also called Cauchy stress, in the constitutive relationship for undamaged material, can be replaced by the effective stress of the damaged material. Thus, a constitutive relationship for frozen soil with damage is obtained:

$$\sigma = (1-D)E\varepsilon. \tag{6}$$

2.3 Evolution of damage

Under an external load, the damage D is supposed to obey

the Weibull distribution. Based on related results for concrete damage [15], the Weibull distribution with double parameters can express the damage quantity D for frozen soil

$$D = 1 - \exp\left[-\left(\frac{\varepsilon}{a}\right)^n\right], \tag{7}$$

where ε is strain, n is the shape parameter and a is the scale parameter, and they are all non-negative numbers. The following equation is deduced from (7):

$$D = 1 - \exp\left[-\frac{1}{n}\left(\frac{\varepsilon}{\varepsilon_f}\right)^n\right]. \tag{8}$$

The expression above is the damage evolution equation in which strain is taken as the damage control variable, ε_f is the strain variable corresponding to the peak stress, and n is a material parameter that represents the evolution of damaged material. Substituting expression (8) into (6) results in a relationship for the constitutive damage of frozen soil:

$$\sigma = E\varepsilon \exp\left[-\frac{1}{n}\left(\frac{\varepsilon}{\varepsilon_f}\right)^n\right]. \tag{9}$$

It can be seen that the stress σ of frozen soil is related to the elastic modulus, ultimate strength, peak stress and its strain. The damage parameter n of frozen soil is a function of the elastic modulus E and the secant modulus E_m. Generally, n is determined by experimental methods or microcosmic mechanics. Theoretically, the n value should be related to the outward failure modes of frozen soil; i.e., frozen soil tends to undergo more brittle failure as n increases, whereas it tends to encounter more plastic failure as n decreases.

2.4 Example calculations

Table 1 presents examples of elastic moduli of soil and ice determined experimentally. By choosing different ice volume contents (c_i), the equivalent elastic modulus of frozen sandy soil under different temperatures are obtained from equations (3) and (4). The porosity ratio e of the frozen soil is 0.4–0.5; natural moisture content (weight %) is 15%–18%.

By utilizing the elastic modulus values of frozen sandy soil under different temperatures as in Table 1 above, stress-strain curves derived from eq. (9) can be constructed as comparisons with experimental data [16] acquired under the same conditions (Figures 1 and 2).

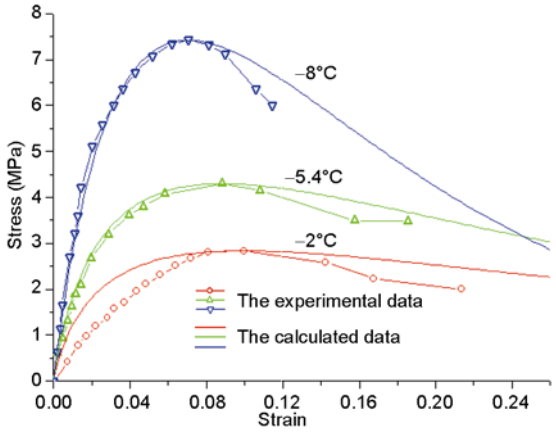

Figure 1 Comparison of the stress-strain curves of frozen sandy soil under different temperatures (κ_i=0.05).

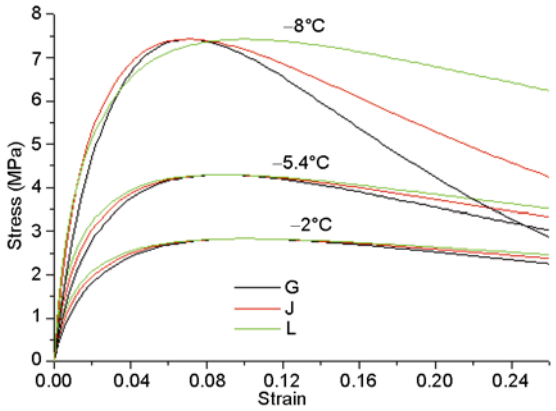

Figure 2 Comparison of the stress-strain curves of damaged frozen sandy soil with different ice contents and under different temperatures(Notes: G—κ_i=0.05; J—κ_i=0.1; L—κ_i=0.2).

Table 1 Equivalent modulus of frozen sand soil under different temperatures

Ice content (%)	Ice temperature (°C)	Elastic modulus of ice (MPa)	Elastic modulus of sandy soil (MPa)	Elastic modulus of frozen sandy soil (MPa)
0.05	–2.0	4910.0	46.0	291.546
	–5.4	6342.0		363.285
	–8.0	6820.0		387.221
0.1	–2.0	4910.0	46.0	534.957
	–5.4	6342.0		678.237
	–8.0	6820.0		726.058
0.2	–2.0	4910.0	46.0	1021.258
	–5.4	6342.0		1307.694
	–8.0	6820.0		1403.303

Comparing the stress-strain curves of frozen sandy soil under different temperatures reveals temperature as an important factor in the deformation of frozen soil. With a decrease in temperature, the unfrozen water content in frozen soil deceases, ice content increases, the cementing bond increases and the deformation of the frozen soil decreases. In addition, with a decrease in frozen soil temperature, the failure form of frozen soil tends to change from rheological behavior and plastic failure to brittle failure. At the same stress level, the deformation of frozen sandy soil decreases with a decrease in soil temperature, whereas the proportion of elastic deformation in total deformation increases. It is also seen that although elastic deformation increases greatly with a decrease in frozen soil temperature, the deformation proportion of the total deformation is very small, especially at higher temperatures (generally > −5°C). The elastic deformation only amounts to 10%–25% of the total (Figures 1 and 2).

To clearly reflect the effect of ice volume percentage (c_i) on the damage strength of frozen soil, we draw the stress-strain curves for various ice contents calculated from eq. (9) for comparison (Figure 2). Under different temperatures, the damage strength of frozen soil is seen to increase with an increase of ice content. However, at the same temperature and with an increase in strain, the compression stress gradually peaks (at the yield point) and then falls. The stress yield points of a range of ice contents in frozen soil tend to converge, showing that the effect of ice content on yield strength is small when frozen soil is fractured.

3 Numerical simulation of three coupled fields (water, temperature and stress)

We here present a numerical simulation of coupled relationships between water, temperature and stress fields using the finite-element routine incorporated with the previously discussed constitutive model. We will show that this numerical simulation results are identical to the practical engineering tests and earlier experimental results.

3.1 The numerical simulation of three fields coupling of channel frozen

3.1.1 Governing differential equations

The hydrothermal coupling transport equation such as a channel in the freezing process can be expressed as a nonlinear parabolic two-dimensional partial differential equation with variable coefficients:

$$\overline{C}\cdot\frac{\partial T}{\partial t}=\frac{\partial}{\partial x}\left(\overline{\lambda}\cdot\frac{\partial T}{\partial x}\right)+\frac{\partial}{\partial y}\left(\overline{\lambda}\cdot\frac{\partial T}{\partial y}\right), \tag{10}$$

where

$$\overline{C}=C+L\cdot\rho_w\cdot\frac{\partial W_u}{\partial T}, \tag{11}$$

$$\overline{\lambda}=\lambda+L\cdot\rho_w\cdot K\frac{\partial W_u}{\partial T}. \tag{12}$$

The relation between the unfrozen water content and temperature can be determined by experiment.

$$W_u=f(T), \tag{13}$$

$$C=\begin{cases}C^+, & T>T_p,\\ \dfrac{1}{2}\cdot(C^++C^-), & T_b\leqslant T\leqslant T_p,\\ C^-, & T<T_b,\end{cases} \tag{14}$$

$$\lambda=\begin{cases}\lambda^+, & T>T_p,\\ \dfrac{1}{2}\cdot(\lambda^++\lambda^-), & T_b\leqslant T\leqslant T_p,\\ \lambda^-, & T<T_b,\end{cases} \tag{15}$$

$$K=0.0036\cdot\exp\big(0.551\cdot(T+0.30)\big), \tag{16}$$

where K, as a transmissibility coefficient, shows exponential decay in a severe phase change zone according to the temperature. The initial condition and boundary condition are:

$$T(x,y,0)=\phi(x,y), \tag{17}$$

$$T(x,0,t)=F_1(t), \tag{18}$$

$$T(x,L_1,t)=F_2(t), \tag{19}$$

$$\frac{\partial T(0,y,t)}{\partial x}=0, \tag{20}$$

$$\frac{\partial T(L_2,y,t)}{\partial x}=0. \tag{21}$$

The above problem is a transient heat conduction subject that takes static temperature field as initial temperature condition on the effect of temperature and water. If the boundary condition of external force and various equations of stress field are considered, especially the constitutive model we developed as physical equation, stress calculation on the effect of temperature and water could be made, namely, the initial coupling calculation of water, thermal and power.

The static balanced equation of channel is

$$[L]\{\sigma\}=0. \tag{22}$$

The geometric equation is

$$\{\varepsilon\} = [L]\{u\}, \tag{23}$$

where,

$$[L] = \begin{bmatrix} \dfrac{\partial}{\partial x} & 0 & 0 & \dfrac{\partial}{\partial y} & 0 & \dfrac{\partial}{\partial z} \\ 0 & \dfrac{\partial}{\partial y} & 0 & \dfrac{\partial}{\partial x} & \dfrac{\partial}{\partial z} & 0 \\ 0 & 0 & \dfrac{\partial}{\partial z} & 0 & \dfrac{\partial}{\partial y} & \dfrac{\partial}{\partial x} \end{bmatrix}. \tag{24}$$

The physical equation (constitutive equation) is

$$\{\sigma\} = [D]\{\varepsilon\} \tag{25}$$

The above equations build up a group of three fields coupling equations which describe temperature, water and stress fields containing a phase change in the frozen soil channel.

3.1.2 The definite condition and the value of each parameter

The volume content of the ice is taken as 0.05, the modulus of elasticity of clay as 12.0 MPa, the modulus of elasticity of ice as 4910.0 MPa and the Poisson's ratio of clay and ice are both 0.3 in calculation.

The initial temperature is –0.3°C on the whole plane. The change of temperature on the upper and lower boundary is expressed as follows:

$$\begin{cases} F_1(t) = -11.2\sin(\pi \cdot t / 3120.0)(d), \\ F_2(t) = 10.9\mathrm{e}^{-0.014(t+336.0)}(d). \end{cases} \tag{26}$$

The computing model is mathematically described by taking the channel soil as an example under bad engineering geology condition [11]. Supposing the outlet is infinitely long, the perpendicular cut face is a flat surface problem, and the soil quality is even and the evaporation heat consumption and other potential fields are ignored. For the channel model, the breadth is 3.0 m, height is 2.0 m, the top channel breadth is 1.0 m, the bottom breadth is 0.5 m and the distance from channel bottom to bottom margin is 1.0 m. The boundary conditions of the model are that direction *X* is free and direction *Y* of lower boundary is limited to moving. Direction *Y* is free and direction *X* of the left-right boundary is limited to moving and directions *X* and *Y* of the upper boundary are free.

The stress boundary conditions show the shear stresses of the left and right boundary are zero. The stress on the upper boundary by channel liner weight and vertical liner frozen force is equal to uniform pressure (*P*=1400 N), whose direction is normal to border line, as shown in Figure 3. For the sake of the contrast, Figure 4 gives a location plan of externally-applied load in the calculation of ref. [5].

The values of each related parameter are taken as follows:

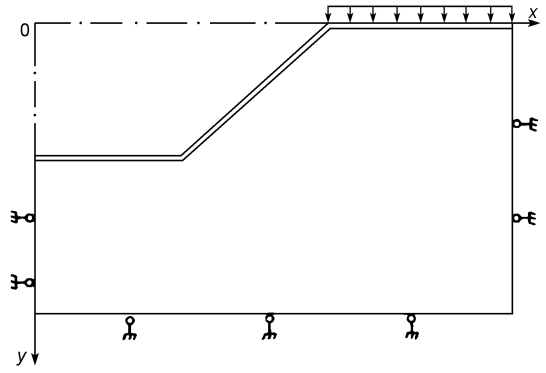

Figure 3 Location where the externally-applied load is during the calculation.

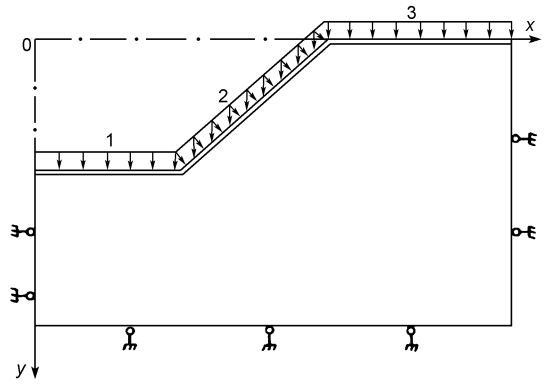

Figure 4 Location where the externally-applied load is applied in ref. [5].

$$C^+ = 3076.7, \quad C^- = 2279.0 \ (\mathrm{kJ\ m^{-3}\ ^\circ C^{-1}}),$$
$$\lambda^+ = 5.53, \quad \lambda^- = 6.58 \ (\mathrm{kJ\ m^{-1}\ h^{-1}\ ^\circ C^{-1}}),$$
$$K_1 = 1.8\times 10^{-0.7},$$
$$K_2 = 0.0036 \cdot \exp(0.551 \cdot (T + 0.30)) \quad (\mathrm{m\ h^{-1}}),$$
$$K_3 = 3.6\times 10^{-3} \quad (\mathrm{m\ h^{-1}}),$$
$$L = 334.7 \ (\mathrm{kJ\ kg^{-1}}),$$
$$T_p = -0.30, \quad T_b = -0.75 \ (^\circ\mathrm{C}),$$
$$W_u = \begin{cases} 0.0664 \cdot \exp(0.0551 \cdot T), & T < -0.75, \\ 0.3058 + 0.596(T + 0.30), & -0.75 \leqslant T \leqslant -0.30, \\ 0.3058, & T > -0.30. \end{cases}$$

3.1.3 The analysis and discussions of the calculated result

The whole model is totally divided into mesh units of 12484 triangles and 6463 nodes by using triangle mesh division. In order to carefully observe the temperature, displacement, stress and strain in the whole frozen process longer time is taken for calculation. The time unit is hour and 2000.0 time units are calculated altogether. The step length is 5.0.

(1) The analysis of temperature field. In channel cutting face, the calculated result of 0°C isotherm distribution in different frozen time periods is shown in Figure 5. The comparison with ref. [5] in Figure 6 demonstrates that 0°C

isotherm distribution is similar in almost the same frozen time.

When frozen for 2000 h, the negative temperature of upper border has reached the max value of −10.12°C, which matches the max value −10.7°C of the upper border negative temperature when frozen for 1536 h calculated from ref. 5. As shown in Figure 7, the temperature changes quickly from the channel slop to the channel bottom, namely, temperature gradient is large. However, the temperature distribution presents an almost parallel straight line under the channel dike far from the channel slop, which is free from the influence of the channel slop boundary temperature. From the temperature field distribution and change, temperature distribution is obviously influenced by a two dimensional boundary, geometry shape of cross section, bottom water replenishment and the heat flow. Compared with the calculation of predecessors, the calculated result of temperature field is satisfactory.

(2) The analysis of displacement field. A great deal of engineering practice has shown that swelling function would happen on the conditions of low frozen speed rate and enough water supplies. Groundwater of higher temperature could reduce frozen speed rate and supply water of frozen front on the channel bottom and channel slop bottom,

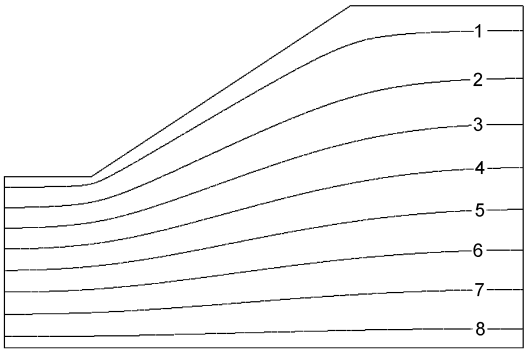

Figure 5 The calculated change of 0ºC isotherm distribution with time. (1–8 are the values of 50, 100, 200, 300, 500, 800, 1000 and 1500 h freezing).

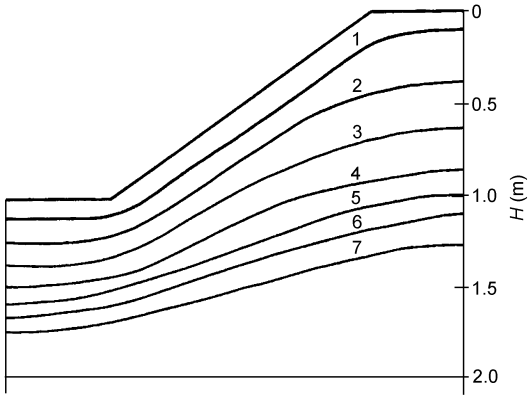

Figure 6 The change of the 0ºC isotherm distribution on document 5. (1–7 are the values of 80, 320, 200, 560, 800, 1040, 1280 and 1600 h frozen).

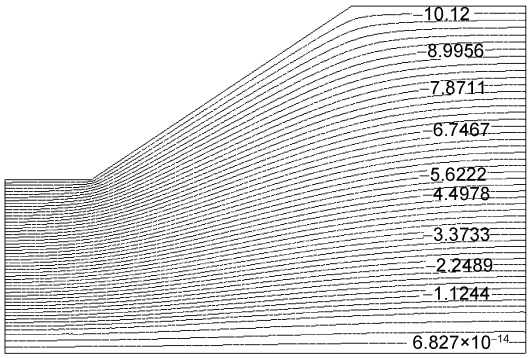

Figure 7 The 0ºC isotherm distribution of 2000 h freezing.

and swelling happens on the channel bottom and channel slop bottom. The swelling displacement distribution ($\sqrt{x^2+y^2}$) is shown in Figure 8 at the point of 2000 h. As shown in Figure 8, the max swelling displacement occurs on the top of channel dike and the upper part of channel slope, and the displacement on the bottom of channel and the lower part of channel slope is also large. Compared with observation data (Figure 9) of the same time, the displacement distribution pattern on the channel cross section is basically consistent.

(3) The analysis of stress field. Figures 10–15 are the contouring distribution graphs of stress σ_x and strain ε_x in the horizontal direction, stress σ_y and strain ε_y in the vertical direction and shear stress τ_{xy} and shear strain γ_{xy} after being frozen for 2000 h. The stress graph shows that the swelling forces on both the bottom of channel and the lower part of channel slope are relatively large and stress concentration

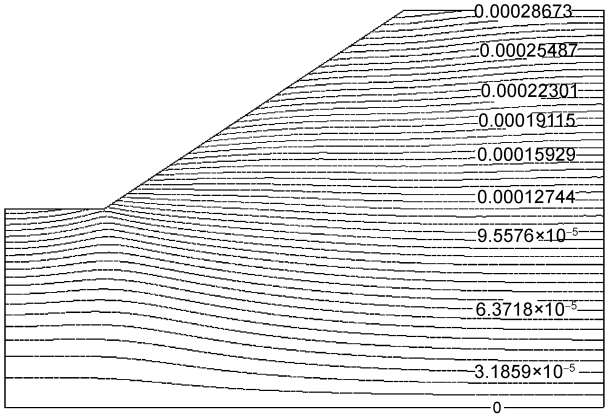

Figure 8 Distribution of the displacement contour of 2000 h freezing.

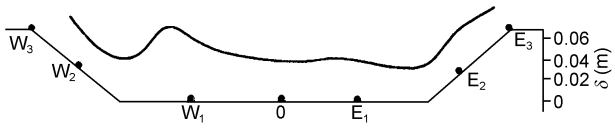

Figure 9 The surface displacement distribution of the Daxin channel working section in Ningxia (running north and south).

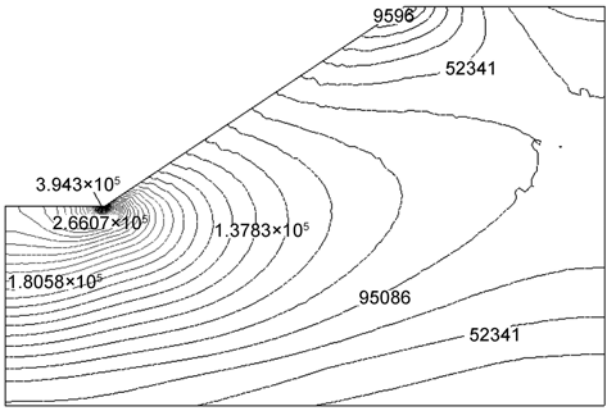

Figure 10 The equal σ_x distribution of 2000 h freezing.

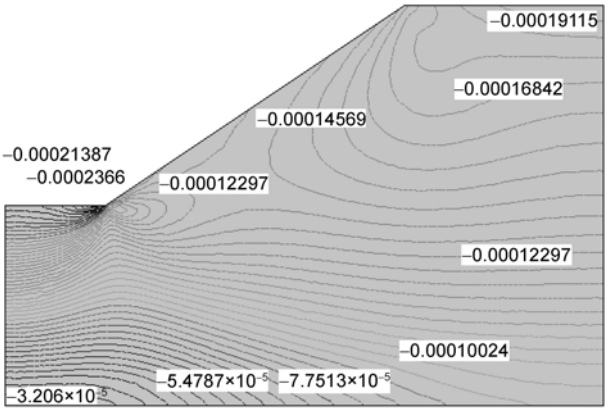

Figure 13 The equal ε_y distribution of 2000 h freezing.

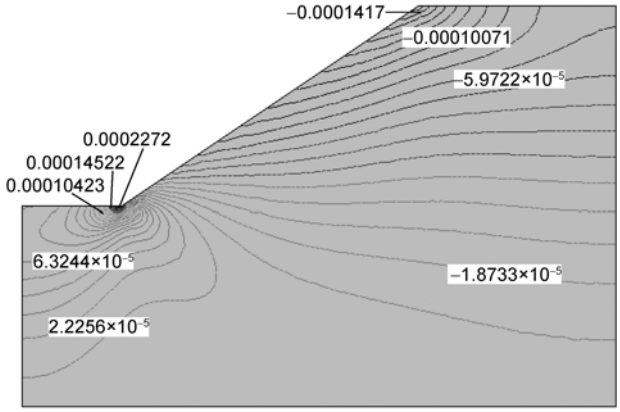

Figure 11 The equal ε_x distribution of 2000 h freezing.

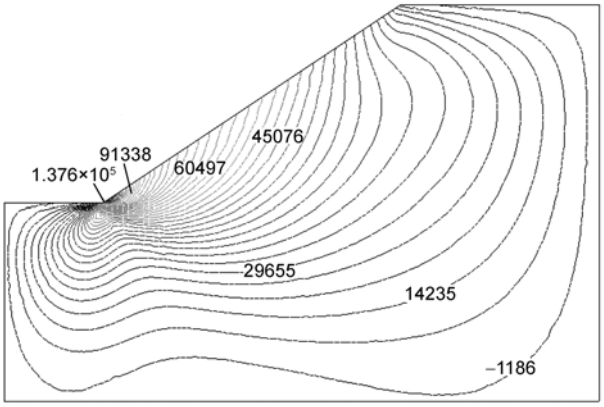

Figure 14 The equal τ_{xx} distribution of 2000 h freezing.

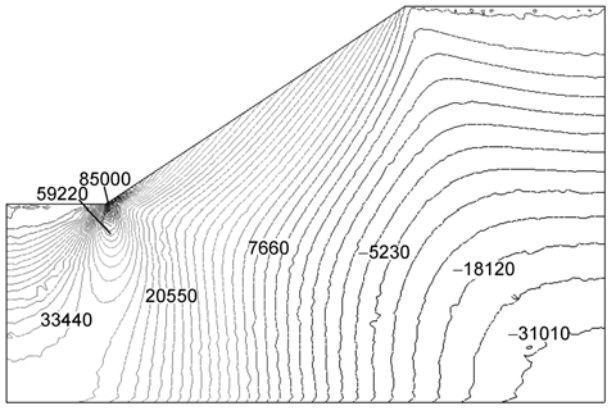

Figure 12 The equal σ_y distribution of 2000 h freezing.

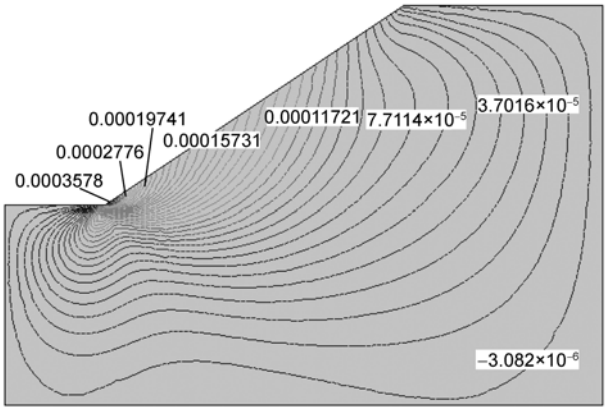

Figure 15 The equal γ_{xx} distribution of 2000 h freezing.

happens at the juncture of channel slope and channel bottom. Meanwhile, the max swelling force also occurs here. The max stress σ_x, σ_y and τ_{xy} are 3.943×10^5 N/m^2, 0.85×10^5 N/m^2 and 1.376×10^5 N/m^2, respectively.

It is also shown that swelling stress is distributed along the direction of height on channel foundation soil. The swelling stress on foundation soil tends to be reduced because of the external load applied on the upper channel foundation soil. With the increase of height, the deformation caused by externally applied load would be reduced and that caused by swelling increased. After exceeding a certain depth, the stress on the foundation soil begins to increase with the increase of height. Therefore, with the increase of height, the stress on foundation soil shows a regular reducing-increasing-reducing pattern, which is the same as the conclusion calculated in ref. [5].

As shown in the above stress-strain distribution figures with different frozen time periods in channel, there is the relationship of one-to-one correspondence between the stress and strain. The equal stress curve tends to change in the same way as the equal strain curve does, which proves the validity of our elastic calculating model.

3.2 The numerical simulation of three fields coupling of the frozen roadbed

3.2.1 Governing differential equations

The controlling differential equation is the same as the previous calculating example, which constitutes three fields coupling equations group in connection with eqs. (22)–(25), which describes temperature, humidity and stress fields in the frozen roadbed.

3.2.2 The definite condition

In this section we analyze the coupling of water, temperature and stress fields within a whole roadbed, consisting of a road dike, side slope and natural surface. The road is assumed to be infinitely long in the longitudinal direction; accordingly, the cross section of the roadbed is treated as a two-dimensional plane in which the distribution of temperatures and stress can be observed. Given the roadbed to be longitudinally symmetrical, only one half of the symmetry needs to be considered in order to reduce the computational complexity and improve the computing precision. For our practical examples, the calculation zone is composed of six homogeneous regions identified as S1, S2, ⋯, S6 (Figure 16), where half of the road dike (region S1, e.g., a cement road surface) is 4.5 m wide (including a road shoulder of 1.0 m width), and 3.0 m high.

(1) Boundary condition. Based on observation data from the Qinghai-Tibet plateau collected over several decades and the boundary layer principle, the definite condition of a fixed boundary is shown as follows [17]:

$$f(t) = T_0 + R_0 t + A_0 \sin\left(\frac{2\pi}{8760} t - \frac{3\pi}{5}\right), \quad (x, y) \in B_1 \cup B_2 \cup B_3, \tag{27}$$

$$\frac{\partial T}{\partial n} = G_s, \quad (x, y) \in B_5, \tag{28}$$

$$\frac{\partial T}{\partial n} = 0, \quad (x, y) \in B_4 \cup B_6, \tag{29}$$

where T_0 is the initial annual average temperature of the base of the lower boundary layer (the measured temperature value of 0.5 m below the ground surface), which agrees with Zang [17] (see Table 2). R_0 is the temperature growth rate of the lower boundary layer bottom caused, potentially, by climate warming. A_0 is the temperature amplitude of the lower boundary layer bottom. n is the exterior normal direction of the border surface. G_s is the geothermal gradient of the lower border of the calculation region. $G_s = 0.03$°C/m.

The displacement boundary conditions of the roadbed model are: the lower boundary B5 limits movement in the y direction but does not limit movement in the x direction. Both the left boundary B4 and the right boundary B6 limit movement in the x direction but do not limit movement in

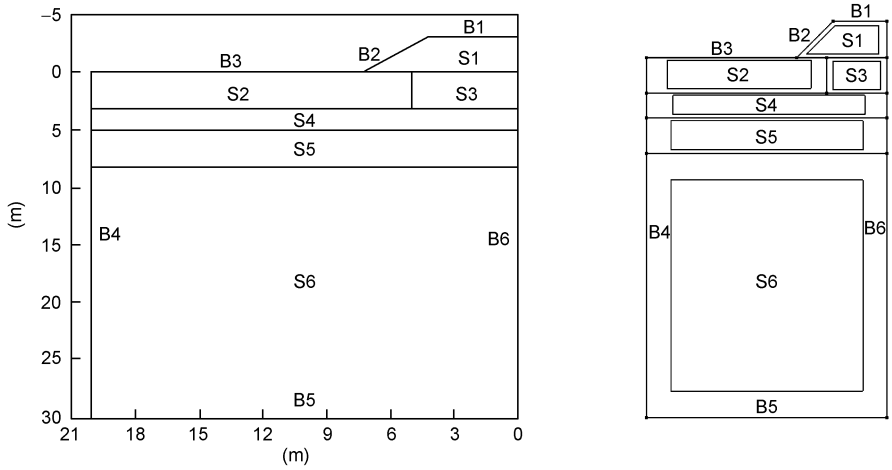

Figure 16 The calculation model of the roadbed temperature field. S1–S6 are the roadbed calculation regions; B1–B6 are the roadbed boundaries.

Table 2 Parameter values of the typical surface boundary layer

Type	Natural surface	Sandy soil side slope	Cement road surface
The total increments of temperature of boundary layer (ºC)	2.5	3.7	4.7

the y direction. Both the x and y directions of the upper boundaries B1, B2 and B3 are free.

The stress boundary conditions are: the shear stress of both the left boundary B4 and the right boundary B6 is 0. The x direction stress on the lower boundary B5 is 0 and there is no load on the upper borders B1, B2 and B3. Therefore, the stress produced in the process of temperature change is heat stress, and the soil coefficient of thermal expansion is 1.0×10^{-5}.

(2) Initial condition. According to the boundary conditions (27)–(29), heat parameters, and the characteristic parameters of the calculation region, we can solve the following Laplace equation:

$$\frac{\partial}{\partial x}\left(\lambda^e\frac{\partial T}{\partial x}\right)+\frac{\partial}{\partial y}\left(\lambda^e\frac{\partial T}{\partial y}\right)=0. \tag{30}$$

Then, we can estimate the temperature field within the calculation region resulting from seasonal thawing.

3.2.3 *The parameter selection*

The calculation region of this example is composed of six kinds of soil (Figure 16) that can be described using practical engineering methods. Exemplary thermal and soil characteristic parameters for these soil types are shown in Table 3. where C is the volumetric heat capacity, λ is thermal conductivity, the subscripts f and u represent the two phase states of freeze and thaw within the roadbed, ρ_d is the dry density, W wt% is the water content and W_u wt% is the unfrozen water content, and D is the water diffusion coefficient. Usually, the water diffusion coefficient of the x direction is assumed to be equal to that of the y direction, i.e., D_x=D_y. The relationship between unfrozen water content and temperature is determined by the following equation [5]:

$$\theta_w=\begin{cases}0.0644\mathrm{e}^{0.0551T}, & T<-0.75,\\ 0.3058+0.596\left(T+0.30\right), & -0.75\leqslant T\leqslant -0.30,\\ 0.3058, & T>-0.30.\end{cases} \tag{31}$$

3.2.4 *Calculation results and the analysis*

The roadbed model (Figure 16) is discretized with a triangular grid for the calculation process. There are a total of 11800 units and 6061 nodes.

(1) Temperature field analysis. By solving Laplace equation (30) based on boundary conditions (27)–(29) and the heat and characteristic parameters of the calculation region, we estimated the temperature field at the time when seasonal thawing starts (Figure 17).

On the basis of the initial temperature distribution obtained by solving the Laplace equation and by taking eq. (27) (R_0=0.0) as the temperature condition of upper boundary changing with time, we repeatedly solved the differential equations over a range of periods. We continued this process until the temperature field under annually changing layer remained stable, and the temperature values above the annually changing layer at the same position and at the same time became identical. At this point, the temperature values of each node were taken as the initial conditions for the three coupled field calculation. The temperature distribution nephogram is shown in Figure 18.

In order to observe the detailed temperature, stress, strain and displacement caused by the freezing process in the roadbed, we ran longer calculations. The time unit used in our calculation was the hour (h), with 2000.0 time units used in total and a time step of 1.0 h. The temperature field shown in Figure 18 is taken as the initial temperature for the whole calculation region.

The following illustrations compare isoline variations for temperature, stress, strain and displacement after the roadbed freezing for 50 h, 500 h, 1000 h and 2000 h, respectively.

From the isotherm distributions (Figures 19–22), showing temperature curves at different time periods after freezing, it can be seen that the internal temperature of the roadbed changes severely during the initial freezing period, because there is a thermal boundary condition varying with time at the upper boundary and heat exchange at the lower boundary. The lowest temperature decreases from –9.229°C to –9.734°C after freezing for 50 h and decreases to –10.24°C after 500 h. The highest temperature drops from 0°C at the beginning to –3.988°C after 500 h. Because the upper boundary is most affected by periodic changes in temperature,

Table 3 Thermal parameters and characteristic parameters of soils for calculation

Soil parameters	S1 gravel and gravelly soil	S2 peat clayey soil	S3 clayey soil containing peat	S4 gravelly clay soil	S5 gravelly clayey soil	S6 weakly weathered bedrock
λ_u (J m^{-1} °C^{-1})	6875.1	3376.7	5110.8	2052.6	3124.2	7164.8
λ_f (J m^{-1} °C^{-1})	9396.0	4684.1	6249.1	3162.1	4376.2	9689.2
C_u (J m^{-3} °C^{-1})	2.183×10^6	2.258×10^6	2.342×10^6	2.166×10^6	2.446×10^6	2.784×10^6
C_f (J m^{-3} °C^{-1})	1.694×10^6	1.781×10^6	1.932×10^6	1.539×10^6	1.932×10^6	2.192×10^6
ρ_d (kg m^{-3})	1800	1200	1400	700	1300	2250
W wt%	10	24	22	56	24	5.6
W_u wt%	3	7	7	20	7	0.6
D	9.35×10^{-6}	1.65×10^{-6}	4.66×10^{-6}	1.21×10^{-6}	3.73×10^{-6}	3.44×10^{-6}

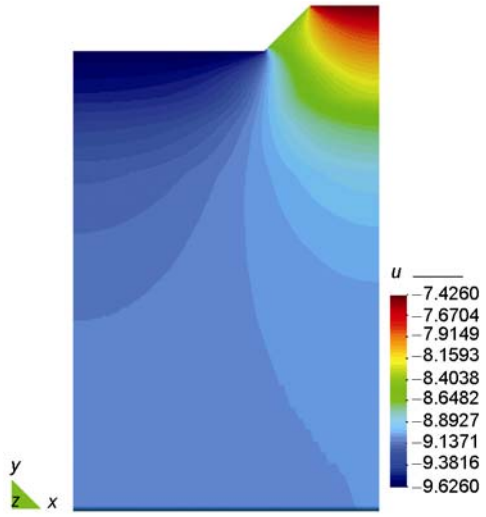

Figure 17 The initial temperature distribution obtained by solving Laplace equation.

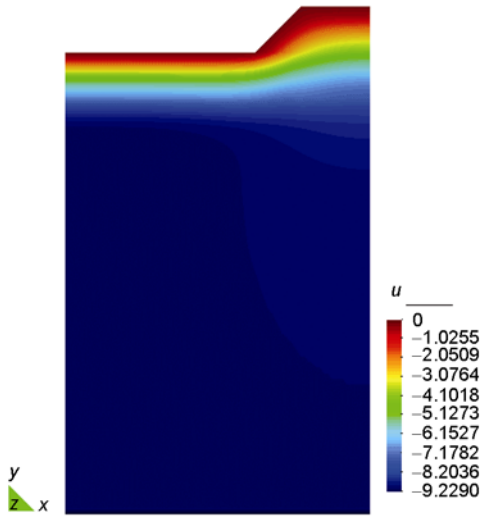

Figure 18 The initial temperature distribution when calculating the three fields coupling.

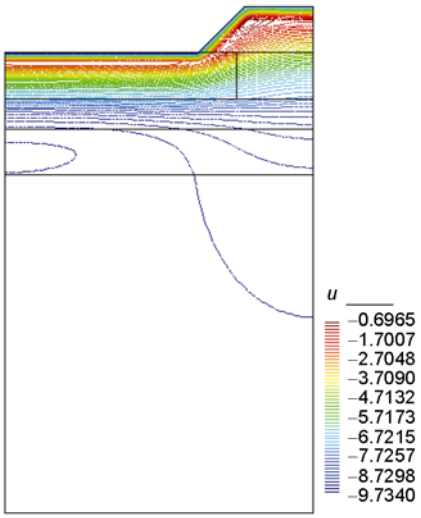

Figure 19 The isotherm distribution for the 50 h freezing.

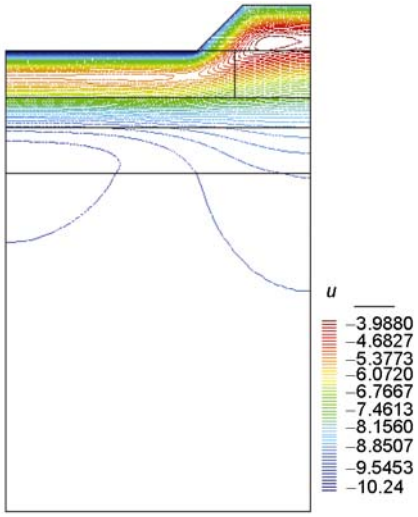

Figure 20 The isotherm distribution for the 500 h freezing.

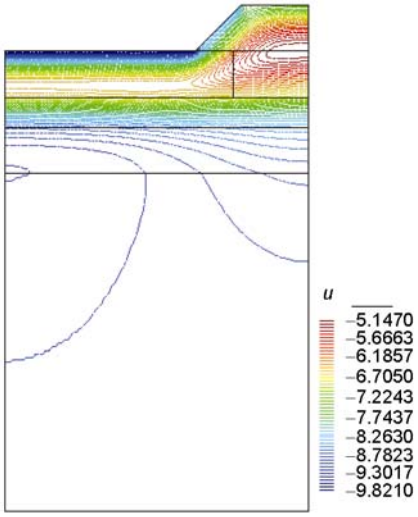

Figure 21 The isotherm distribution for the 1000 h freezing.

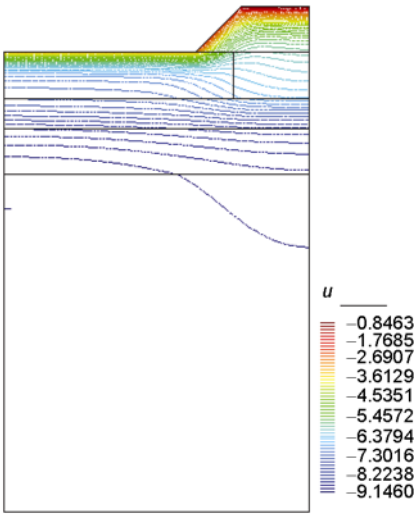

Figure 22 The isotherm distribution for the 2000 h freezing.

the internal temperature of the roadbed rises again after some time. The lowest temperature rises from −10.24°C after freezing for 500 h to −9.821°C after 1000 h and −9.145°C after 2000 h. In addition, it can be seen from the variation of the whole temperature field that the regions where temperature varies the greatest within the roadbed are all shallower than 5.0 m–6.0 m beneath the natural surface in the upper part of the roadbed. Temperatures do not change greatly below these depths. The depth of 1.0 m–3.0 m beneath the natural surface is the region with the most frequent and distinct temperature variation; i.e., this region is usually identified as a phase transition zone between water and ice. These phenomena are in accordance with observational results of practical engineering applications. Generally, the Earth's surface influenced by seasonal and climatic temperature variations on the surface is limited to the upper 5 to 10 m. Areas deeper than this are almost always free from the influence of Earth surface temperature change.

(2) Displacement field analysis. Because the roadbed model is free from external loads when calculating the three coupled fields, the stress, strain and displacement must therefore all be produced by frost heave and thaw collapse. As shown in Figures 23 and 24, the greatest displacement in the horizontal (x) direction produced during the freezing process is 0.0002853 m and −0.000472 m in the vertical (y) direction, which shows that the deformation in the horizontal direction produced by frost heave is a little smaller than in the vertical direction.

(3) Stress field analysis. Figures 25 and 26 are nephograms that show the greatest stress. The greatest stress in the horizontal (x) direction produced during the freezing process is about 1.81×10^5 Pa and about 0.4974×10^5 Pa in the vertical (y) direction. The stress in the horizontal direction is more than three times of that in the vertical direction.

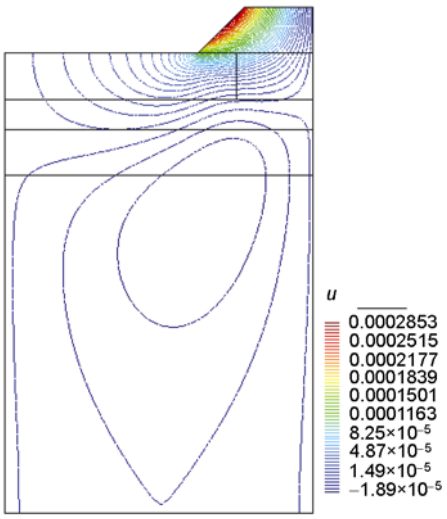

Figure 23 The equal displacement distribution of the x direction after the 2000 h freezing.

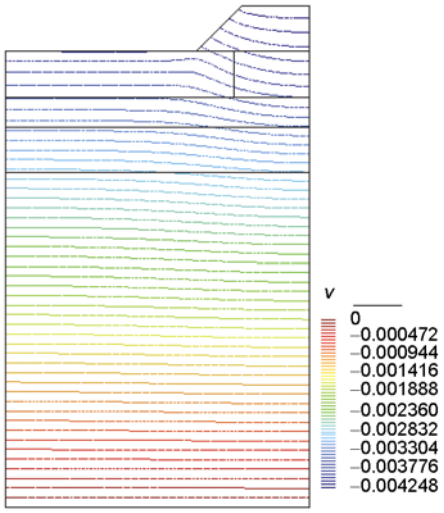

Figure 24 The equal displacement distribution of the y direction after the 1000 h freezing.

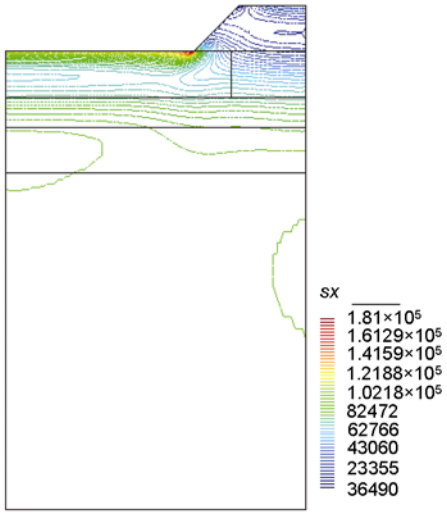

Figure 25 The equal σ_x distribution after the 500 h freezing.

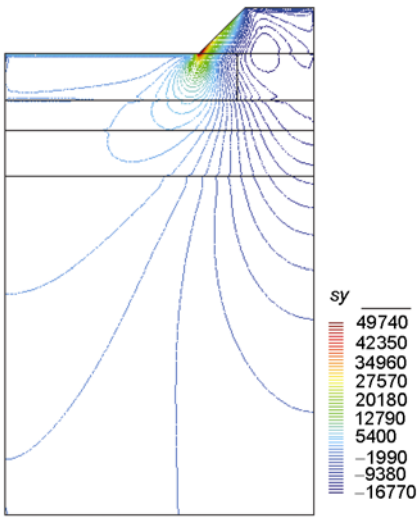

Figure 26 The equal σ_y distribution after the 500 h freezing.

This is because the displacement in the horizontal direction is limited in the calculation. The greatest stresses in both the horizontal and vertical directions also appear at the same period, which occurs because the stress and deformation of the frozen soil roadbed vary with periodic variations in the boundary temperature. Again, the area that is mostly influenced by atmospheric temperature boundary conditions is within a depth of 6.0 m of the natural Earth surface. The influence is smaller in the region deeper than 6.0 m.

In order to clarify the calculated results, eight specific points within the roadbed were selected for closer study. The first of these is at a depth of 1.5 m beneath the top roadbed, and the other seven were distributed every 1.5 m along the same line. Variations in temperature, displacement, stress and strain over time were observed. For the whole freezing-thawing process, the changes of each physical quantity under a depth of 10.0 m from the natural earth surface are so small that we only display points shallower than 12.0 m in Figure 27.

Comparisons of the calculated results for the eight points are shown in Figures 28–31.

From the curves of the eight points' temperature, displacement, stress and strain changing with time, we can see that, in the first several years, the maximum thawing depth of frozen soil within the roadbed in the vertical direction increases quickly and gradually stabilizes because of the effect of the heat storage within the internal roadbed. Five or six years after completion of the roadbed, the influence of the temperature field is relatively small, and the temperature field varies more slowly in the deeper parts of the internal roadbed, which agrees with the observed results from practical engineering applications.

The closer the observation point is to the roadbed top, the greater the temperature, displacement, stress and strain change, which indicates that the changes from external conditions can have a great effect on the shallow Earth surface. This also illustrates that in practical construction processes, higher embankments will result in a shallower upper limit to natural frozen soil and a greater thawing depth for frozen soil within the embankment. This will reduce the influence of external construction and protect naturally frozen soil in permafrost regions. However, in practical construction, increasing the height of an embankment may not be eco-

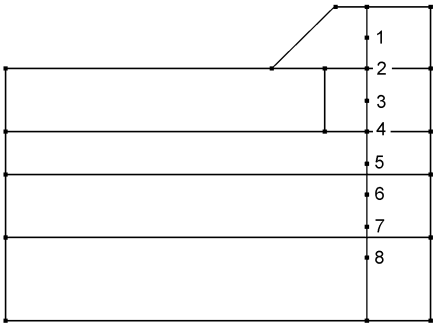

Figure 27 The position sketch of the eight special points.

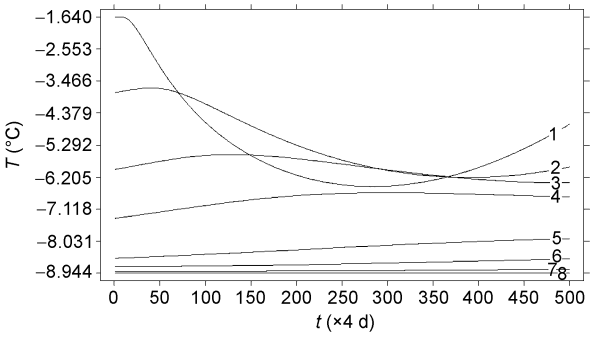

Figure 28 The curves of temperature changing with time.

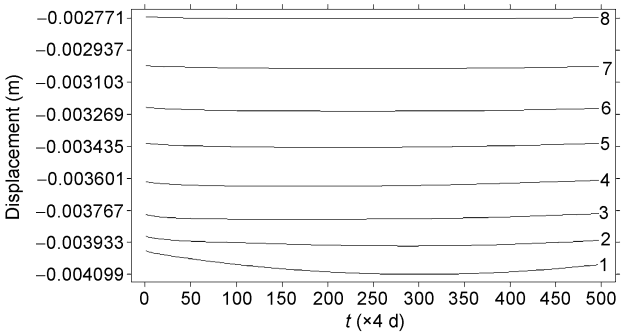

Figure 29 The curves of displacement changing with time in the *y* direction.

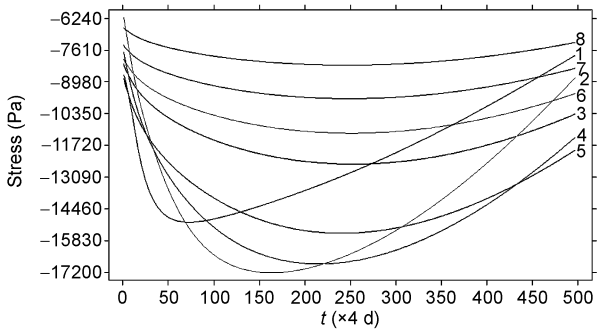

Figure 30 The curves of stress changing with time in the *y* direction.

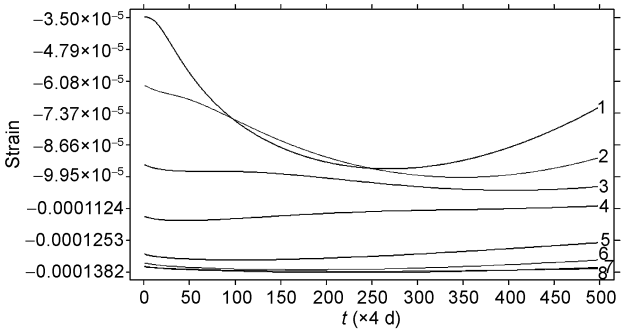

Figure 31 The curves of strain changing with time in the *y* direction.

nomical. This could be overcome by choosing a material with poor heat conductivity to cover the surface of the embankment. Alternatively, a thermal insulting layer could be laid on the embankment to prevent the influence of external temperature change on naturally frozen soil, and to assure the stability of the natural upper limit of the frozen soil.

The stress of the point nearest the upper roadbed surface varies greatly because of the influence of external temperatures and humidity. However, the stress and strain of the eight points all tend to change in a similar fashion, which suggests that our elastic constitutive model describes frozen roadbed conditions well.

4 Conclusions

(1) The relationships between the elastic constants of soil, ice, and the composite frozen soil body over a range of temperatures have been established. On this basis, the method of damage mechanics has been applied to frozen soil mechanics research, and a new frozen soil constitutive model with damage has been presented.

(2) The result of computing is consistent with the result of predecessors and the actual test result, and the regulations are alike. The computing result has shown that the swelling stress is distributed along the direction of channel foundation depth, and tends to fade away because of the stipulate function of the external load on the upper channel foundation.

(3) The calculated result from three fields coupling of frozen foundation has shown that the districts in which temperature varies violently inside the roadbed flat are all within the scope of the whole upper roadbed part with the depth of natural 5.0 m–6.0 m apart from earth's surface. The temperature does not vary obviously in most districts under this depth. Under the earth surface about the depth scope of 1.0 m–3.0 m there is a district with more multifarious and violent temperature variety. It is usually called the violent phase change district, in which the phase change transformation between water and ice occurs because of freezing and melting.

This research was supported by the National Natural Science Foundation of China (Grant No. 10625208) and the National Basic Research Program of China (Grant No. 2010CB832700 6).

1 Fremond M, Mikkola M. Thermomechanical of freezing soil. In: Proceedings of the Sixth International Symposium on Ground Freezing. Rottendam: A. A. Balkema, 1991. 57–66
2 Gary P, Jason W. A model for freeze-thaw cycling of the South Pole Station exterior sheathing. Cold Regions Sci Technol, 2008, 52: 254–261.
3 Konrad J, Duquennoi C. A model for water transport and ice lensing in freezing soils. Water Resour Res, 1993, 29: 3109–3124
4 Dennis E, Pafahl A. Frost Action. Section 3 of Roads and Airfields in Cold Regions. Edited by Teds Vinson. Washington: Washington State University Press, 1996. 51–85
5 An W D, Wu Z W, Ma W, et al. Interaction among Temperature Moisture and Stress Fields in Frozen Soil (in Chinese). Lanzhou: Lanzhou University Press, 1989. 78–95
6 Foriero A, Ladaryi B, Dallimore R, et al. Modelling of deep seated hill slope creep in permafrost. Can Geotech J. 1998, 35: 560–578
7 Su B, Li N, Quan X J. The numerical study on the ventilated embankment in permafrost regions in Qinghai–Tibet railway. Cold Regions Sci Technol, 2004: 229–238
8 Dempsey B. A mathematical model for predicting coupled heat and water movement in unsaturated soil. Int J Numer Anal Methods Geomech, 1978: 19–34
9 Rai M, Roegiers J C. Fluid flow and heat flow in deformable fractured porous media. Int J Eng Sci, 1994: 1615–1633
10 Masters I, Pao W K, Lewis R W. Coupling temperature to a double-porosity model of deformable porous media. Int J Numer Methods Eng, 2000: 421–438
11 Zhang M Y, Lai Y M, Gao Z H, et al. Influence of boundary conditions on the cooling effect of crushed-rock embankment in permafrost regions of Qinghai–Tibetan Plateau. Cold Regions Sci Technol, 2006, 44: 225–239
12 Ning J G, Wang H, Zhu Z W. Investigation of the constitutive model of frozen soil based on meso-mechanics (in Chinese). Trans Beijing Inst Technol, 2005, 25: 847–851
13 Lemaitre J, Chaboche J L. Mechanics of Solid Materials. London: Cambridge University Press, 1990. 159–168
14 Du S Y, Wang B. Meso-Mechanics of Composite Materials (in Chinese). Beijing: Science Press, 1989. 43–47
15 Wu Z. Investigation of concrete tensive and compressive constitutive model based on damage mechanics (in Chinese). Water Resour Hydropower Eng, 1995, 11: 58–63
16 Wu Z W, Ma W. The strength and creep of permafrost. Lanzhou: Lanzhou University Press, 1994. 125–127
17 Zang E M, Wu Z W. Long time degeneration of frozen soil road engineering (in Chinese). Lanzhou: Lanzhou University Press, 1999. 94–103